Strong-field processes induced by an ultrashort linearly polarized pulse with two carrier frequencies

D. Habibović [1] and D. B. Milošević [1,2]

[1] *Faculty of Science, University of Sarajevo, Zmaja od Bosne 35, 71000 Sarajevo, Bosnia and Herzegovina*

[2] *Department of Natural and Mathematical Sciences, Academy of Sciences and Arts of Bosnia and Herzegovina, Bistrik 7, 71000 Sarajevo, Bosnia and Herzegovina*

(Received 14 February 2024; accepted 27 March 2024; published 11 April 2024)

We perform a detailed semianalytical study of the characteristics of strong-field processes induced by an ultrashort linearly polarized pulse with two carrier frequencies. We show that the photoelectron spectra depend to a great extent on the absolute phases of the field components and on the duration of the pulse. By using the saddle-point method, we show that this dependence can be exploited to control the electron dynamics in the laser field. Besides the photoelectron spectra, we also investigate the spectra of high-order harmonics. Again, we find a strong dependence on the absolute phases and the duration of the pulse. We present the spectra using a false color scale in the absolute phase-harmonic energy plane, and show that particular regions in this plane can be assessed using the simple man's model founded on the classical solution of the Newton equation of motion. Finally, we investigate the symmetry properties of the photoelectron and high-order harmonic spectra with respect to the transformation which includes the change of the absolute phase, and compare them with those valid for a long driving pulse with a flat envelope.

DOI: 10.1103/PhysRevA.109.043110

I. INTRODUCTION

When an atom or molecule is exposed to an intense laser field many processes can be induced. Among these, particularly interesting are high-order above-threshold ionization (HATI) and high-order harmonic generation (HHG) (for review see [1–9]). For both of these processes, following the ionization of the atom or molecule by the strong laser field, the released electron is propagated in the continuum. The oscillatory laser field may return the electron in the vicinity of the parent ion, and then various scenarios may happen. For HATI, the electron rescatters off the parent ion, while the scenario which corresponds to the HHG assumes that the electron is recombined with the parent ion and the energy excess is released in the form of the high-order harmonic. This simple picture is called the three-step model [10,11].

The simplest case of the driving field is a monochromatic field which can be represented as an infinitely long pulse with a flat envelope. During the past three decades, a rapid development of the laser technologies made possible the construction of more complex near-infrared lasers with the pulses which consist of only a small number of optical cycles [12]. These pulses allow one to record the electron dynamics in real time [13] and they are called the few-cycle pulses. The corresponding electric field can be written in the form of the product of the carrier wave and the envelope function. The phase between the maximum of the envelope and the nearest maximum of the carrier wave is called the absolute phase or the carrier-envelope phase (CEP). The influence of the CEP on the photoelectron emission was reported in the experiment [14] and was theoretically explained in [15] for the laser pulses with nonstabilized CEP. Later, the technological advancements enabled construction of the CEP-stabilized laser systems for which the influence of the CEP on the photoelectron emission was investigated both experimentally [16] and theoretically [17]. An example of experimental and theoretical investigations of molecular HATI induced by a few-cycle pulse is given in [18]. The influence of the exact value of the CEP on the ionization of atoms and molecules by the circularly polarized field was investigated in [19], while the theory which allows one to extract the CEP dependence of observables using the wave function for a single value of the CEP was presented in [20]. Besides the above-threshold ionization, the HHG process also depends on the value of the CEP [21–27], as well as the other strong-field processes such as nonsequential double ionization [28–32], dissociation [33,34], laser-assisted electron-atom scattering [35], and laser-assisted electron-ion radiative recombination [36]. Moreover, the characteristics of different atomic and molecular processes in a linearly polarized few-cycle field were analyzed in [37]. Finally, the plasmonic field-enhanced HHG and its dependence on the CEP was investigated in [38].

Apart from the CEP, the characteristics of HATI and HHG spectra also depend on the other laser-field parameters and the specificities of the atomic or molecular target [39,40]. In order to achieve particularly advanced control of the process, the so-called tailored laser fields are useful. The examples of the long pulses with a flat envelope include the bichromatic linearly polarized field, the bicircular field, and the orthogonally polarized two-color field. The bichromatic linearly

polarized field consists of two linearly polarized components with mutually parallel polarizations, while the bicircular field has two circularly polarized components. The orthogonally polarized two-color field has two linearly polarized components but, contrary to the case of the bichromatic linearly polarized field, the polarizations of these components are mutually perpendicular. For these driving fields, HATI and HHG spectra depend on the frequencies of both field components and the relative phase between them. For a few-cycle pulse, additional parameters appear and they can be used to control the process. More specifically, the spectra depend on the duration or length of the pulse (i.e., on the number of optical cycles per pulse), the CEP, and the shape of the envelope. For example, the ionization of argon atoms induced by an ultrashort linearly polarized field with two carrier waves was investigated in [41] both theoretically and experimentally. Here, the duration of the pulses of the two waves was not equal. Furthermore, the ionization of neon atoms by the linearly polarized femtosecond pulse, which consists of the XUV and infrared components, was explored in [42]. Also, the linearly polarized pulse with two carrier frequencies and a time delay between the two components was employed in [43] to analyze the possibility of optimization of the HHG intensity and the position of the cutoff. More recently, the possibility of extraction of the phase and time delays of attosecond wave packets formed in strong-field ionization was theoretically investigated using a two-carrier linearly polarized femtosecond field with one strong and one weak component [44]. Also, the subcycle electron dynamics during the strong-field ionization of NO molecules was investigated using a similar driving pulse [45]. Apart from the gaseous media, the ultrashort pulses have many applications in the solid-state physics. For example, using the two ultrashort lasers, the dynamics of the electrons in the bulk alpha quartz was investigated with the time-dependent density functional theory [46].

In order to model HATI and HHG processes, various theories can be employed. The most accurate theories rely on the solution of the time-dependent Schrödinger equation [47,48]. These calculations are time consuming even for the simple atoms or molecules and the semianalytical approaches are beneficial. Particularly prominent examples of these approaches are the theories based on the strong-field approximation (SFA) which assumes that the interaction between the liberated electron and the parent ion is negligible during the electron propagation in the continuum. The Coulomb interaction between the liberated electron and the parent ion can be included in the calculations [49–51], but this contribution usually remains small [52]. We have already applied our SFA-based theory to investigate various characteristics of HATI and HHG spectra induced by the long tailored laser fields [39,53–56]. More recently, we have explored the characteristics of the processes induced by the few-cycle driving fields with two carrier frequencies [57,58]. For the linearly polarized few-cycle pulse, we have found that the agreement between the results obtained using our SFA theory and the theory based on the time-dependent Schrödinger equation is excellent in the high-energy part of the spectra for both the HATI and HHG processes [38,59–61]. We expect the same to be valid for the driving pulses with two carrier frequencies.

In the present contribution, we analyze the dependence of HATI and HHG spectra on the parameters of the few-cycle linearly polarized pulse with two carrier frequencies. The paper is organized as follows. In Sec. II, we briefly present the SFA-based theory of the HATI and HHG processes induced by the few-cycle linearly polarized pulse. Also, we briefly discuss the saddle-point method which allows one to get an insight into the underlying physics of the process. The calculated numerical results are presented in Sec. III, while the main discussions and conclusions are given in Sec. IV. Atomic units are used unless otherwise stated.

II. THEORY

In this section we briefly present the SFA-based theory of HATI and HHG processes. Also, we succinctly discuss the saddle-point method and the simple man's model.

A. HATI theory

The differential ionization probability for transition from the initial bound state ψ_m to the final continuum state, which corresponds to the photoelectron with asymptotic momentum $\mathbf{p}$, is $W_{\mathbf{p}} = p\sum_m |M_{\mathbf{p}m}|^2$ where $p = |\mathbf{p}|$ is the momentum amplitude, the sum over m is the sum over the magnetic quantum number, and $M_{\mathbf{p}m}$ is the probability amplitude given by $M_{\mathbf{p}m} = M^{(0)}_{\mathbf{p}m} + M^{(1)}_{\mathbf{p}m}$, with [61]

$$M^{(0)}_{\mathbf{p}m} = -i\int_0^{\tau_p} dt_0 \boldsymbol{\mathcal{M}}_m(\tilde{\mathbf{p}}, t_0)\cdot\mathbf{E}(t_0)e^{iS(\tilde{\mathbf{p}},t_0)}, \tag{1}$$

$$M^{(1)}_{\mathbf{p}m} = \int_0^{\tau_p} dt e^{iS(\tilde{\mathbf{p}},t)}\int_0^t dt_0\left[\frac{2\pi}{i(t-t_0)}\right]^{3/2}\langle\tilde{\mathbf{p}}|V|\mathbf{k}_{\rm st}\rangle \times e^{-iS(\mathbf{k}_{\rm st};t,t_0)}\boldsymbol{\mathcal{M}}_m(\mathbf{k}_{\rm st}, t_0)\cdot\mathbf{E}(t_0). \tag{2}$$

Here $M^{(0)}_{\mathbf{p}m}$ is the contribution of the direct electrons, i.e., the electrons which after liberation go directly to the detector without further interaction with the parent ion. On the other hand, $M^{(1)}_{\mathbf{p}m}$ is the contribution of the rescattered electrons, which after the liberation interact once with the core. Also, $\tilde{\mathbf{p}} = \mathbf{p} - \mathbf{A}(\tau_p)$, $\mathbf{A}(t) = -\int^t \mathbf{E}(t')dt'$ being the vector potential of the applied field $\mathbf{E}(t)$; $\tau_p = n_p T$ is the pulse length expressed as an integer multiple of the laser period T, $\mathbf{k}_{\rm st} = -\int_{t_0}^t dt'\mathbf{A}(t')/(t-t_0)$ is the stationary momentum, and t_0 and t are the ionization and rescattering times, respectively. Also, $\boldsymbol{\mathcal{M}}_m(\mathbf{q}, t_0) = \langle\mathbf{q} + \mathbf{A}(t_0)|\mathbf{r}|\psi_m\rangle$ is the ionization matrix element, while $S(\tilde{\mathbf{p}}, t_0) = I_p t_0 + \int^{t_0} dt'[\tilde{\mathbf{p}} + \mathbf{A}(t')]^2/2$ and $S(\mathbf{k}_{\rm st}; t, t_0) = \int_{t_0}^t dt'\{[\mathbf{k}_{\rm st} + \mathbf{A}(t')]^2/2 + I_p\}$ are the actions of the direct and rescattered electrons, respectively. Finally, I_p is the ionization potential of the bound state which we represent by a linear combination of the Slater-type orbitals

$$\psi_m \equiv \psi_{lm}(\mathbf{r}) = \sum_a C_a\frac{(2\zeta_a)^{n_a+1/2}}{\sqrt{(2n_a)!}}r^{n_a-1}e^{-\zeta_a r}Y_{lm}(\Omega). \tag{3}$$

Here, $Y_{lm}(\Omega)$ are the spherical harmonics, n_a, l and m are the quantum numbers, while the coefficients C_a and ζ_a are tabulated in [62]. Finally, the rescattering potential $V(r)$ is modeled by the double Yukawa potential [63]. Besides the double Yukawa potential, a more accurate rescattering potential, which includes six parameters instead of two, can also be

used as the rescattering potential [64,65]. However, this potential leads to almost the same results as our double Yukawa potential except in the low-energy part of the spectrum [64].

The integrals which appear in the probability amplitude $M_{\mathbf{p}m}^{(1)}$ can be solved numerically, or by using the saddle-point method. In the latter approach, the stationarity of the action $S(\tilde{\mathbf{p}}, t_0) - S(\mathbf{k}_{\rm st}; t, t_0)$ with respect to t_0 and t leads to the saddle-point equations

$$[\mathbf{k}_{\rm st} + \mathbf{A}(t_0)]^2 = -2I_p,$$
$$[\tilde{\mathbf{p}} + \mathbf{A}(t)]^2 = [\mathbf{k}_{\rm st} + \mathbf{A}(t)]^2, \tag{4}$$

with the complex solutions for t_0 and t. Then, the probability amplitude $M_{\mathbf{p}m}^{(1)}$ can be written as a sum of the contributions of different saddle-point solutions (see Appendix B in [61]).

B. HHG theory

For the HHG process, the intensity of the harmonic with frequency $\Omega_{\mathbf{K}}$ and wave vector $\mathbf{K}$ is $I_{\Omega_{\mathbf{K}}} \propto \Omega_{\mathbf{K}}^4 |\mathbf{T}_{\Omega_{\mathbf{K}}}|^2$, where the T-matrix element $\mathbf{T}_{\Omega_{\mathbf{K}}}$ is

$$\mathbf{T}_{\Omega_{\mathbf{K}}} = \int_0^{\tau_p} \frac{dt}{T} \sum_m \mathbf{d}_m(t) e^{i\Omega_{\mathbf{K}} t}, \tag{5}$$

and the sum over m is the sum over the magnetic quantum number of the bound state. The time-dependent dipole is [2,66]

$$\mathbf{d}_m(t) = -i \int_{-\infty}^{t} dt_0 \left[\frac{2\pi}{i(t-t_0)}\right]^{3/2} \boldsymbol{\mathcal{M}}_m^*(\mathbf{k}_{\rm st}, t) \times e^{-iS(\mathbf{k}_{\rm st}; t, t_0)} \boldsymbol{\mathcal{M}}_m(\mathbf{k}_{\rm st}, t_0) \cdot \mathbf{E}(t_0), \tag{6}$$

where the time t now represents the recombination time. Besides the ionization matrix element $\boldsymbol{\mathcal{M}}_m(\mathbf{k}_{\rm st}, t_0)$, the recombination matrix element $\boldsymbol{\mathcal{M}}_m^*(\mathbf{k}_{\rm st}, t)$ appears as well. Here we only consider the atoms with closed electron shells so that the magnetic quantum number of the initial and final states is the same [66].

Important insight into the strong-field process can be gained by exploring the electron dynamics described by the Newton equation for an electron exposed to the laser field. This is the foundation of the simple man's model introduced in [67–69] and applied to the three-step processes in [10,11,70]. The optimal harmonic intensity is determined by the condition that the electron velocity at the ionization time is zero. Using this condition, we obtain that the harmonic intensity is maximal for the harmonic-photon energy [54]:

$$\Omega_{\mathbf{K},\rm opt} = I_p + [\mathbf{A}(t) - \mathbf{A}(t_0)]^2/2. \tag{7}$$

In this paper as the driving field we use a few-cycle linearly polarized pulse with two carrier frequencies. This field can be presented as

$$\mathbf{E}(t) = f(t)[E_1 \sin(r\omega t + \varphi_1) + E_2 \sin(s\omega t + \varphi_2)]\hat{\mathbf{e}}_x, \tag{8}$$

where E_j and φ_j with $j = 1, 2$ are the electric-field amplitudes and absolute phases, $\omega = 2\pi/T$ is the fundamental carrier frequency, r and s are integers, and $f(t) = \sin^2[\omega t/(2n_p)]$ for $t \in [0, \tau_p]$; $f(t) = 0$ otherwise is the pulse envelope. The real vector $\hat{\mathbf{e}}_x$ defines the driving-field polarization direction.

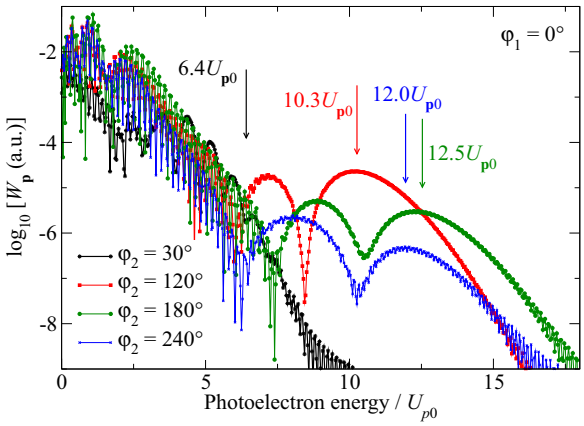

FIG. 1. Logarithm of the differential ionization probability as a function of the photoelectron energy of Ar for HATI induced by the ω-2ω linearly polarized few-cycle pulse with the component intensity $E_1^2 = E_2^2 = 10^{14}\,\mathrm{W/cm^2}$, fundamental carrier wavelength of 800 nm, and the values of the absolute phases as indicated in the panel. The total pulse duration and the emission angle are $\tau_p = 4T$ and $\theta_e = 0^\circ$, respectively.

III. NUMERICAL RESULTS

In order to investigate the characteristics of HATI and HHG spectra induced using the pulse given by Eq. (8), we use the example of the Ar atom. The corresponding ionization potential is $I_p = 15.76$ eV and its ground state is modeled using two $2p$ and two $3p$ states for which $n_a = 2$, $l = 1$, $m = 0, \pm 1$ and $n_a = 3$, $l = 1$, $m = 0, \pm 1$, respectively.

A. High-order above-threshold ionization

We start our investigations by exploring the dependence of the HATI spectrum on the values of the absolute phases and the length of the pulse. The emission angle θ_e is defined as the angle between the final photoelectron momentum and the axis defined by $\hat{\mathbf{e}}_x$. In Fig. 1 we present the photoelectron spectra induced by the ω-2ω linearly polarized few-cycle ($n_p = 4$) pulse with component intensity $E_1^2 = E_2^2 = 10^{14}\,\mathrm{W/cm^2}$, fundamental carrier wavelength of 800 nm, and the values of the absolute phases as indicated in the panel. For our driving field, we fix the value of the phase $\varphi_1 = 0^\circ$ and change the phase φ_2. The photoelectron energy is expressed in units of $U_{p0} = [E_1^2/(r\omega)^2 + E_2^2/(s\omega)^2]/4$, $r = 1$, $s = 2$, and the emission angle is $\theta_e = 0^\circ$. The photoelectron spectrum depends to a great extent on the value of the absolute phase. This is particularly true for the position of the cutoff (see the arrows in Fig. 1). For example, for the absolute phase $\varphi_2 = 30^\circ$, the emission of the medium- and high-energy electrons is significantly suppressed and the cutoff appears for the energy around $6.4U_{\mathbf{p}0}$. On the other hand, for the values of the absolute phase $\varphi_2 > 60^\circ$, the rescattering plateau extends to a much higher energy [see the red (cutoff at $10.3U_{\mathbf{p}0}$), green (cutoff at $12.5U_{\mathbf{p}0}$), and blue (cutoff at $12.0U_{\mathbf{p}0}$) arrows in Fig. 1 for the values of the absolute phase $\varphi_2 = 120^\circ$, 180°, and 240°, respectively]. Besides the position of the cutoff, the value of the differential ionization probability also depends on the absolute phase in the sense that the height of the rescattering plateau strongly depends on this parameter. For example, for

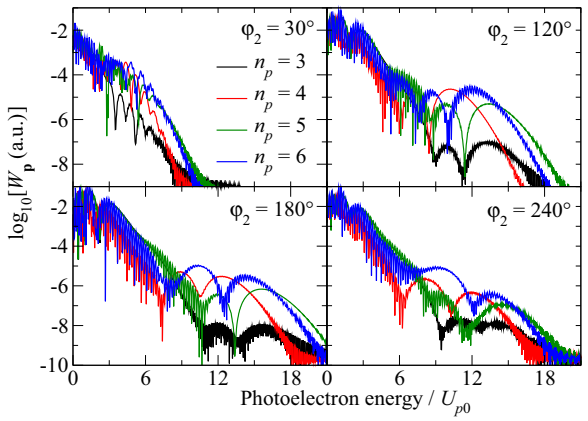

FIG. 2. Logarithm of the differential ionization probability as a function of the photoelectron energy of Ar for HATI induced by the ω-2ω linearly polarized few-cycle pulse which consists of n_p optical cycles, as indicated in the upper left panel, and for the values of the absolute phase φ_2 as indicated in the panels. Other driving-field parameters and the emission angle are the same as in Fig. 1.

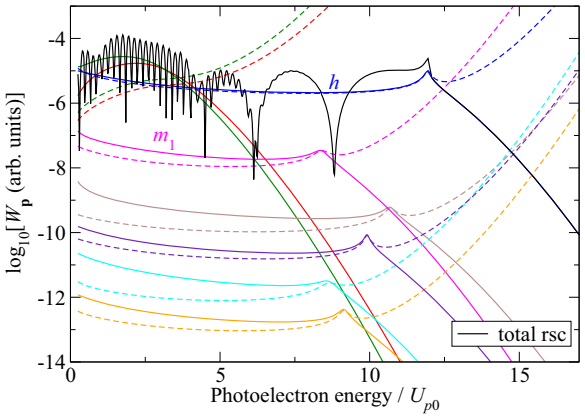

FIG. 3. Saddle-point partial contributions to the differential ionization probability for the driving pulse with $\varphi_2 = 120^\circ$ and the same other parameters as in Fig. 1. The pair which is dominant in the high-energy part of the spectrum is denoted by h, while the pair whose contribution is significant in the medium part of the spectrum is denoted by m_1.

the photoelectron energy ($E_\mathbf{p} = \mathbf{p}^2/2$) $E_\mathbf{p} > 6U_{\mathbf{p}0}$, the HATI spectra are significantly different for different values of the absolute phase. The plateau is the longest for $\varphi_2 = 180^\circ$. Also, for $\varphi_2 < 180^\circ$ ($\varphi_2 > 180^\circ$) the photoelectron yield is higher (lower) than the corresponding yield obtained for $\varphi_2 = 180^\circ$. In order to gain full information about the dependence of the photoelectron spectra on the absolute phase, it is necessary to investigate this dependence together with the dependence on the length of the pulse. For this purpose, in Fig. 2 we present the photoelectron yield obtained using the same driving pulse as in Fig. 1 but with n_p optical cycles per pulse, as indicated in the upper left panel, and for the values of the phase φ_2 as indicated in the panels. The phase φ_1 is zero. The length and height of the rescattering plateau strongly depend on the pulse duration. As a rule, for a very short laser pulse (which covers only three optical cycles), the photoelectron yield is lower than that for pulses with more than three optical cycles (see the upper right and lower left panels in Fig. 2). The only exception is for the phase φ_2 around 240°. In this case the photoelectron emission is also suppressed for longer pulses even though not to such an extent as for the case with $n_p = 3$ (see the lower right panel of Fig. 2).

The fact that the medium- and high-energy parts of the photoelectron spectrum are suppressed for certain interval of values of the phase φ_2 can be elaborated using the saddle-point method. The partial contributions to the differential ionization probability, which correspond to the solutions of the saddle-point equations (4) and significantly contribute to the spectrum, are displayed in Fig. 3 for the driving pulse with the phase $\varphi_2 = 120^\circ$ and the same other parameters as in Fig. 1. Similarly as for the driving pulse with one carrier frequency, the solutions appear in pairs [61] and the contributions of the solutions which diverge after the cutoff should be discarded (dashed lines in Fig. 3) [71,72]. The contributions of the direct electrons are not presented in Fig. 3. For the given values of the driving-pulse parameters, the medium- and high-energy parts of the spectrum are solely determined by the partial contributions denoted by h and m_1 [see the blue (h) and magenta (m_1) solid and dashed lines in Fig. 3]. The low-energy region of the spectrum is dominated by the direct electrons [cf. the red (gray; cutoff at $10U_{\mathbf{p}0}$) line in the upper right panel of Fig. 2 with the black solid line in Fig. 3; they coincide very well except in the low-energy part of the spectrum]. The number of saddle-point solutions significantly increases with the increase of the length of the pulse. However, the number of the saddle-point solutions which lead to the significant contributions to the differential ionization probability remains relatively small. In order to analyze how the partial contributions to the differential ionization probability depend on the value of the absolute phase φ_2, it is enough to investigate how the pairs denoted by h and m_1 behave as functions of this parameter. For this purpose, in Fig. 4 we present the complex ionization time for the pairs of solutions of the saddle-point equations which contribute significantly in the high-energy (left panel) and medium-energy (right panel)

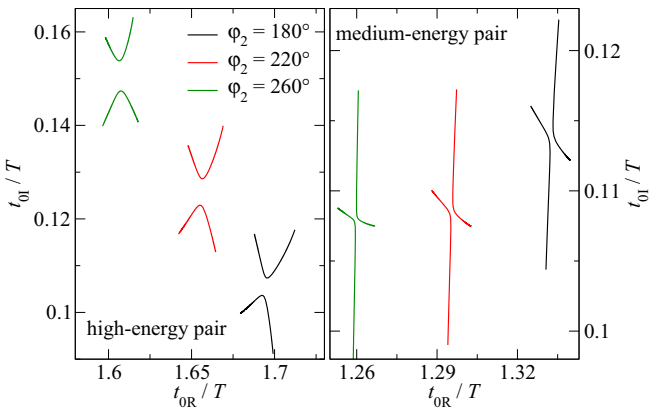

FIG. 4. Complex saddle-point solutions for the high-energy (left panel) and medium-energy (right panel) pair for the driving pulse with the absolute phase $\varphi_2 = 180^\circ$ (black lines; largest t_{0R}), $\varphi_2 = 220^\circ$ (red lines; medium t_{0R}), and $\varphi_2 = 260^\circ$ (green lines; smallest t_{0R}), and the same other parameters as in Fig. 1.

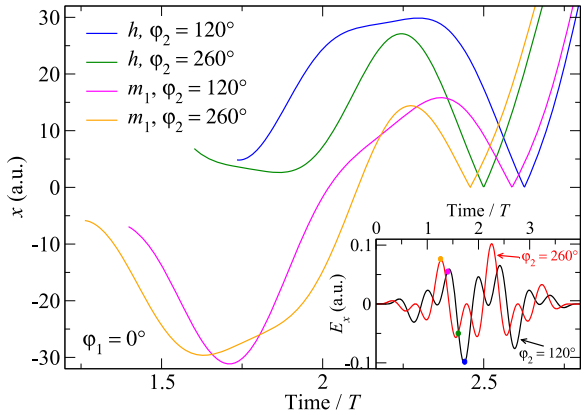

FIG. 5. Photoelectron trajectories for the convergent solutions of the h [blue and green (upper) lines] and m_1 [magenta and orange (lower) lines] pairs of the saddle-point solutions for the absolute phase as indicated in the panel. The photoelectron energy is $E_{\mathbf{p}} = 7.5U_{p0}$. Other pulse parameters are the same as in Fig. 1. Inset: The electric field for the two values of the phase as indicated in the panel, and with the relevant real part of the ionization times denoted by dots.

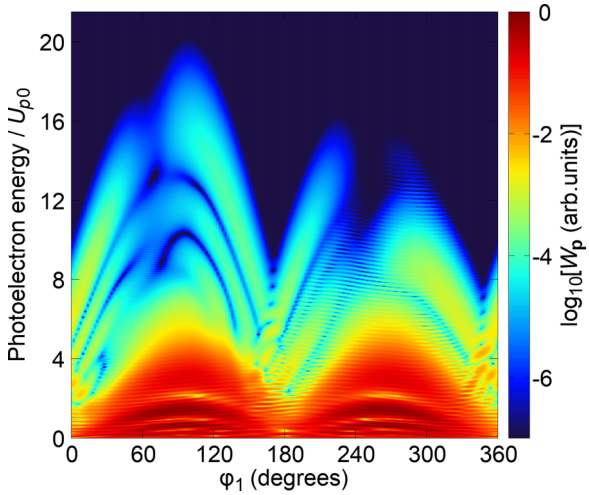

FIG. 6. Logarithm of the differential ionization probability as a function of the absolute phase φ_1 and the photoelectron energy for the driving pulse with $\varphi_2 = 0^\circ$ and the same other parameters as in Fig. 1.

parts of the spectrum, for the values of the phase φ_2 as indicated in the left panel and the same other field parameters as in Fig. 1. The imaginary part of the ionization time $t_{0\mathrm{I}}$ is related to the ionization probability in such a way that the increase of $t_{0\mathrm{I}}$ corresponds to the exponential decrease of the ionization probability. With this in mind, it is easy to see that the contribution of the high-energy (medium-energy) solution decreases (increases) with the increase of the phase φ_2. More precisely, for $\varphi_1 = 0^\circ$, as the phase φ_2 increases from $\varphi_2 = 120^\circ$ towards $\varphi_2 = 260^\circ$, the partial contribution of the pair h (m_1) to the differential ionization probability becomes smaller (larger). For the pair h, this change is particularly pronounced for $\varphi_2 \in [180^\circ, 260^\circ]$. Apart from the pairs h and m_1, contributions of other saddle-point solutions remain negligible regardless of the values of the absolute phases.

This behavior can successfully be exploited to control the electron dynamics using the absolute phase as the parameter. The quantum orbits are defined as the solutions of the Newton equation of motion for the electron in the laser field for complex ionization and rescattering times [61,73]. The photoelectron trajectories are given by the real part of $\mathbf{r}(t') = \mathbf{k}_{\mathrm{st}}(t' - t_0) + \boldsymbol{\alpha}(t') - \boldsymbol{\alpha}(t_0)$ for $\mathrm{Re}\, t_0 \leqslant t' \leqslant \mathrm{Re}\, t$, and $\mathbf{r}(t') = \mathbf{p}(t' - t) + \boldsymbol{\alpha}(t') - \boldsymbol{\alpha}(t)$, for $t' > \mathrm{Re}\, t$, where $\boldsymbol{\alpha}(t) = \int^t \mathbf{A}(t')dt'$ is the electron excursion in the laser field. In Fig. 5 we present the photoelectron trajectories for the energy $E_{\mathbf{p}} = 7.5U_{p0}$ and for the convergent contributions of the h [blue and green (upper) lines] and m_1 [magenta and orange (lower) lines] pairs of the saddle-point solutions for the absolute phase as indicated in the legend. The inset in Fig. 5 displays the electric field as a function of time for the two values of the absolute phase as indicated in the panel. For $\varphi_2 = 120^\circ$, the medium-energy and high-energy parts of the spectrum are exclusively determined by the solutions of the h pair so that, for this value of the absolute phase, the electron motion in the laser field would be as shown by the blue (uppermost) line in Fig. 5. The corresponding real part of the ionization time is denoted by the blue dot in the inset. Clearly, the ionization happens when the electric field is close to its maximal value, thus leading to the significant differential ionization probability. For the value $\varphi_2 = 260^\circ$, the situation is different. Namely, the ionization time for the h solution is slightly changed with respect to the one obtained with $\varphi_2 = 120^\circ$ (see the green dot in the inset), but the field strength is radically different and the contribution of this solution becomes negligible. The situation is opposite for the m_1 solution, which is significant for $\varphi_2 = 260^\circ$ [compare the positions of the magenta and orange (upper) dots with the positions of the blue and green (lower) dots in the inset]. The electron trajectory which corresponds to this solution is very different with respect to the one obtained for the h solution. In this way, by changing the absolute phase, we can achieve that only one, out of two pairs of solutions, is dominant, thus attaining a fine control of the motion of the released electron. For a few-cycle pulse with only one carrier frequency, far less advanced control is possible. Besides the dependence of the spectra on the second-harmonic absolute phase, it is also instructive to investigate how the photoelectron yield depends on the absolute phase φ_1 of the carrier field. In Fig. 6 we present the logarithm of the differential ionization probability as a function of the absolute phase φ_1 and the photoelectron energy for the ω-2ω driving pulse with $\varphi_2 = 0^\circ$ and the same other parameters as in Fig. 1. The position of the cutoff and the value of the differential ionization probability strongly depend on the absolute phase φ_1. For example, for the values of the φ_1 slightly smaller than π and 2π, the cutoff appears for the photoelectron energy $E_{\mathbf{p}} < 7U_{p0}$, while for the phase $\varphi_1 \approx 100^\circ$, the position of the cutoff appears for $E_{\mathbf{p}} > 16U_{p0}$. In addition, the spectra do not possess any nontrivial symmetry properties with respect to the change of the phase φ_1. Besides the position of the cutoff, the dependence of the differential ionization probability on the photoelectron energy also depends to a significant extent on the phase φ_1. For example, for $\varphi_1 \approx 120^\circ$, the spectrum exhibits relatively smooth structure with only two deep minima, while for $\varphi_1 \approx 240^\circ$,

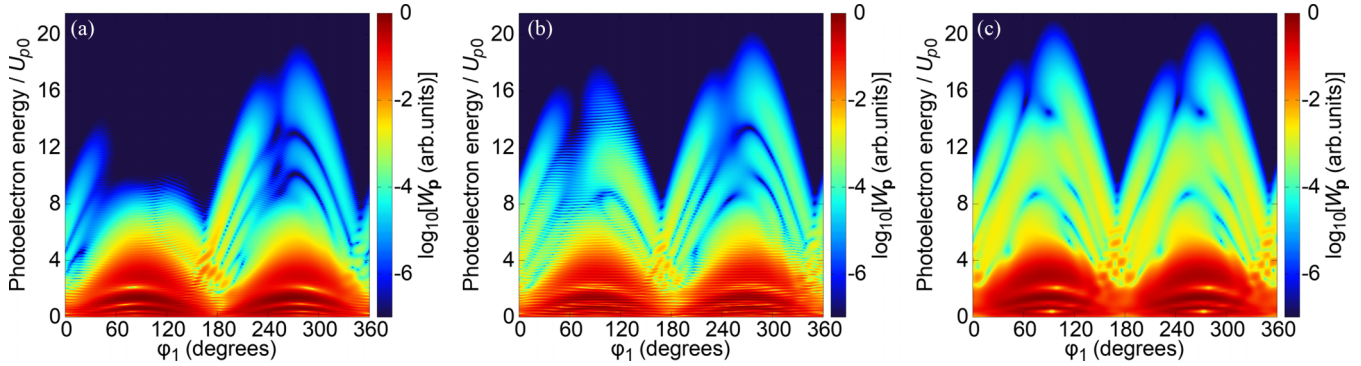

FIG. 7. Logarithm of the differential ionization probability as a function of the absolute phase φ_1 and the photoelectron energy for the driving field with $n_p = 3$ (a) and $n_p = 5$ (b) optical cycles per pulse, and for the long pulse with a flat envelope (c). The absolute phase is $\varphi_2 = 0^\circ$ and the other parameters are as in Fig. 1.

the photoelectron yield exhibits almost erratic behavior as a function of the photoelectron energy.

Now we analyze how the dependence of the differential ionization probability on the absolute phase φ_1 is changed as a function of the pulse length. For that purpose, in Fig. 7 we present the logarithm of the differential ionization probability as a function of the absolute phase φ_1 and the photoelectron energy for the driving field with $n_p = 3$ [panel (a)] and $n_p = 5$ [panel (b)] optical cycles per pulse, and for the long pulse with a flat envelope [panel (c)]. Other parameters are the same as in Fig. 6. By comparing the results displayed in Fig. 6 and in Figs. 7(a) and 7(b) with the results shown in Fig. 7(c), it becomes clear that the length of the pulse has a big impact on the photoelectron spectra. If a long pulse with a flat envelope [$f(t) = 1$ in Eq. (8)] is employed to induce the process, the photoelectron spectra exhibit a symmetry $W_{\mathbf{p}}(\varphi_1, \varphi_2) = W_{\mathbf{p}}(\varphi_1 + \pi, \varphi_2)$ (see the Appendix). For an ultrashort pump pulse, this symmetry is broken and the photoelectron spectra significantly depend on the value of the absolute phase φ_1. For example, for the driving pulse with $n_p = 3$ optical cycles, the emission of the high-energy electrons is suppressed for $\varphi_1 < \pi$, while those electrons are present for $\varphi_1 > \pi$ [see Fig. 7(a)]. In contrast, for the driving pulse with $n_p = 4$ optical cycles, the high-energy electrons are predominantly emitted for $\varphi_1 < \pi$, and are suppressed for $\varphi_1 > \pi$ (see Fig. 6). Finally, for $n_p \gtrsim 5$, the symmetry with respect to the change $\varphi_1 \to \varphi_1 + \pi$ becomes more apparent [see Fig. 7(b)] even though it is exact only for a long pulse with a flat envelope [see Fig. 7(c)]. It is also interesting to mention that, for the ω-2ω long pulse with a flat envelope, the symmetry with respect to the change $\varphi_2 \to \varphi_2 + \pi$ does not exist. Consequently, with a fixed phase φ_1 and changing the phase φ_2 we can only get one broad region of the phase φ_2 for which the high-energy electrons are expected with a significant ionization probability. On the other hand, with a fixed phase φ_2 and changing the phase φ_1 we get two regions of the phase φ_1 for which the high-energy electrons are expected with a significant probability. The discussed symmetries can be derived using the dynamical symmetry of the field as explained in [39] (for more details see the Appendix). For a few-cycle pump, the mentioned symmetries can only be approximate and they cannot be observed at all if the number of optical cycles per pulse is very small ($n_p < 5$).

Let us now, using the saddle-point method, discuss the suppression of the emission of the high-energy electrons for some values of the phase φ_1. In Fig. 8 we present the logarithm of the differential ionization probability as a function of the photoelectron energy calculated by numerical integration (black solid lines) and by using the saddle-point method [red (gray) solid lines], together with the partial contributions of different saddle-point solutions. The spectra calculated using the saddle-point method do not include the contributions of the direct electrons, while they are included in the spectra calculated by numerical integration. The values of the absolute phases (in all panels it is $\varphi_2 = 0^\circ$) and the number of optical cycles per pulse are denoted in the panels. For the four-cycle pulse, the high-energy part of the spectrum is determined by one pair of the saddle-point contributions [blue lines (with the highest cutoff) in Figs. 8(a) and 8(b)]. However, for $\varphi_1 = 120^\circ$, these contributions are pronounced, while for $\varphi_1 = 240^\circ$ they are suppressed by approximately two orders of magnitude. Because there are no other contributions to the high-energy part of the spectrum, the photoelectron emission would be suppressed for φ_1 around 240° (in accordance with the results shown in Fig. 6). Furthermore, the medium-energy part of the spectrum ($6U_{p0} < E_{\mathbf{p}} < 10U_{p0}$) is also affected by the change of the phase φ_1. For example, for $\varphi_1 = 120^\circ$ this part of the spectrum is determined by the high-energy solutions and only one additional solution [green solid line (disappears from the panel at $10U_{\mathbf{p}0}$) in Fig. 8(a)] so that the total spectrum remains relatively smooth. On the other hand, for $\varphi_1 = 240^\circ$ the medium-energy part of the spectrum is determined by many saddle-point solutions [see the magenta, orange, cyan, and blue (different shades of gray) lines in Fig. 8(b)], thus exhibiting erratic oscillations of the total yield.

The discussion is much simpler for an even shorter pulse. For the three-cycle pulse, the number of the relevant saddle-point solutions is much smaller than for the four-cycle pulse. The rescattered yield is usually determined by only one pair of the saddle-point contributions. Consequently, if the contribution of that pair of the saddle-point solutions is suppressed for some values of the absolute phase, the whole yield is also expected to be suppressed. For example, for $\varphi_1 = 120^\circ$ (and other values of φ_1 close to this one), the rescattering is almost completely absent [see the black, red (gray), and brown (light gray; uppermost) lines in Fig. 8(c); the contribution

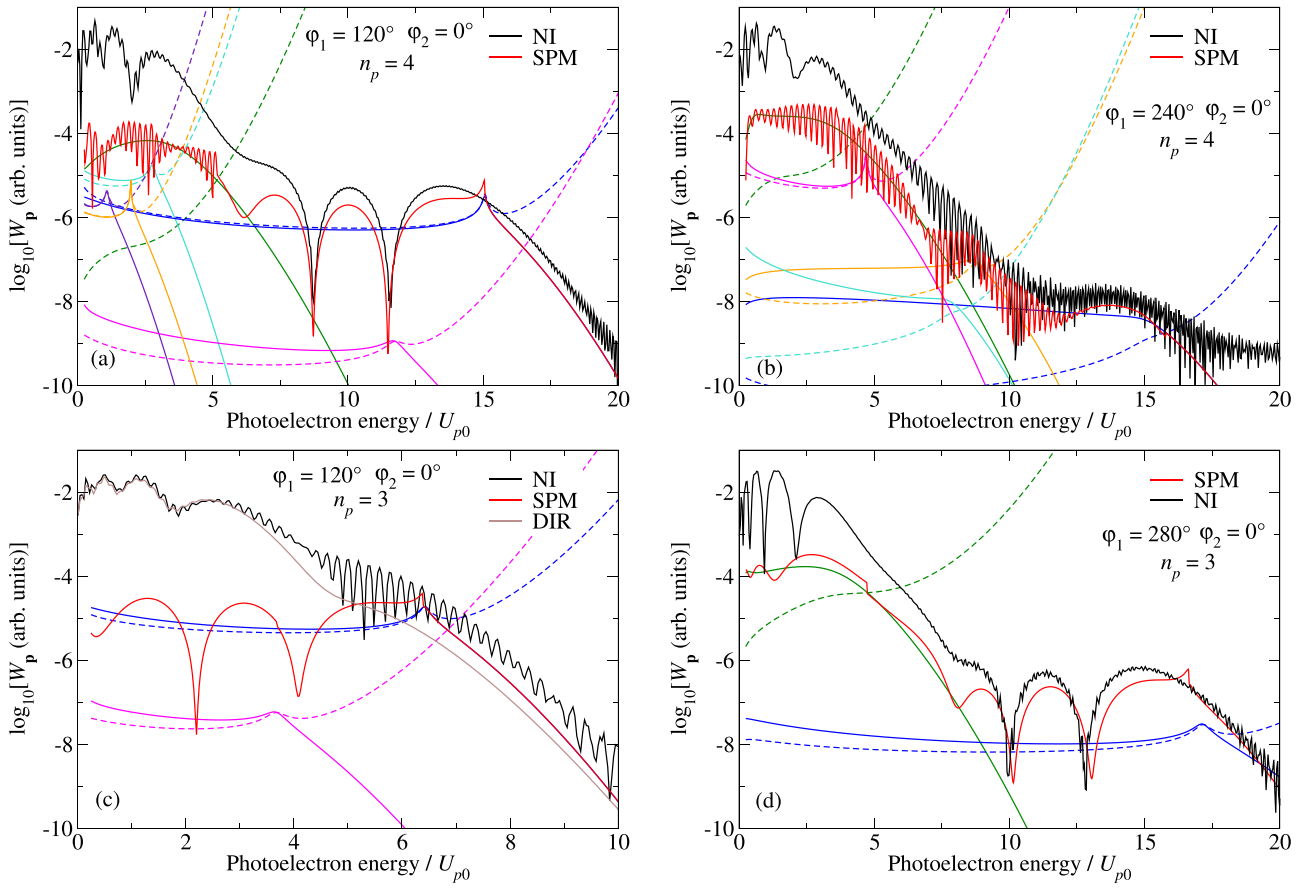

FIG. 8. Logarithm of the differential ionization probability as a function of the photoelectron energy calculated by numerical integration (black solid lines) and by using the saddle-point method [red (gray) solid lines], together with the contributions of different saddle-point solutions. The spectra calculated using the saddle-point method do not include the contributions of the direct electrons, while they are included in the spectra calculated by the numerical integration. The values of the absolute phases and the number of optical cycles per pulse are denoted in the panels. Other parameters are the same as in Fig. 1.

of the direct electrons is denoted by the brown (light gray; uppermost) line]. The rescattering pair of the saddle-point contributions [blue (dark gray) lines in Fig. 8(c)] is relevant only in the narrow region around $6U_p$ where it is of the same order of magnitude as the contribution of the direct electrons. This explains the strong suppression of the yield for high energies and near $\varphi_1 = 120^\circ$ in Fig. 7(a). On the other hand, for $\varphi_1 = 280^\circ$ (and other values close to this one) the contribution of the rescattering pair extends to $E_{\mathbf{p}} > 16U_{p0}$ and the rescattering plateau is well pronounced. Finally, it is worth mentioning that the obtained photoelectron spectra are very different in comparison with the spectra generated using the pulse with one carrier frequency. For example, the position of the cutoff for the process induced by a one-carrier field is close to $10U_{p0}$, while for the two-carrier driving pulse, the photoelectrons can have much higher energy, depending on the values of the absolute phases.

B. High-order harmonic generation

After analyzing HATI by the linearly polarized few cycle pulse with two carrier frequencies, we now investigate the characteristics of the HHG process induced by this pulse. First, we explore the dependence of the harmonic yield on the absolute phase φ_1, for the fixed value of the phase φ_2. When HHG is induced by a long bichromatic field with a flat envelope, the length of the HHG plateau and the value of the harmonic intensity significantly depend on the value of the phase φ_1. However, the harmonic yield is invariant with respect to the transformation $\varphi_1 \to \varphi_1 + \pi/2$ (see the Appendix). For example, for the phase $\varphi_2 = 0^\circ$, the length of the plateau would be the shortest for $\varphi_1 = 25^\circ + j \times 90^\circ$, where j is an integer, while the longest plateau can be expected for $\varphi_1 = 67^\circ + j \times 90^\circ$. In the former case, the cutoff appears close to $3.2U_{p0}$, while in the latter case, it is at a much higher energy close to $5U_{p0}$. The symmetry with respect to the change $\varphi_1 \to \varphi_1 + \pi/2$ is broken when a few-cycle pulse is employed to induce the process. Consequently, the characteristics which appear in the harmonic yield due to the short nature of the pump pulse can easily be examined by comparing the harmonic yields calculated for the driving pulse with the phase $\varphi_1 + j\pi/2$, j being an integer. In Fig. 9 we present the logarithm of the harmonic intensity as a function of the harmonic energy for the Ar atom exposed to the three-cycle ω-2ω linearly polarized field with the absolute phases $\varphi_2 = 0^\circ$ and φ_1 as indicated in the panels. The intensity of the driving-field components is $E_1^2 = E_2^2 = 10^{14}\,\mathrm{W/cm^2}$, while the fundamental carrier wavelength is 1600 nm. We have

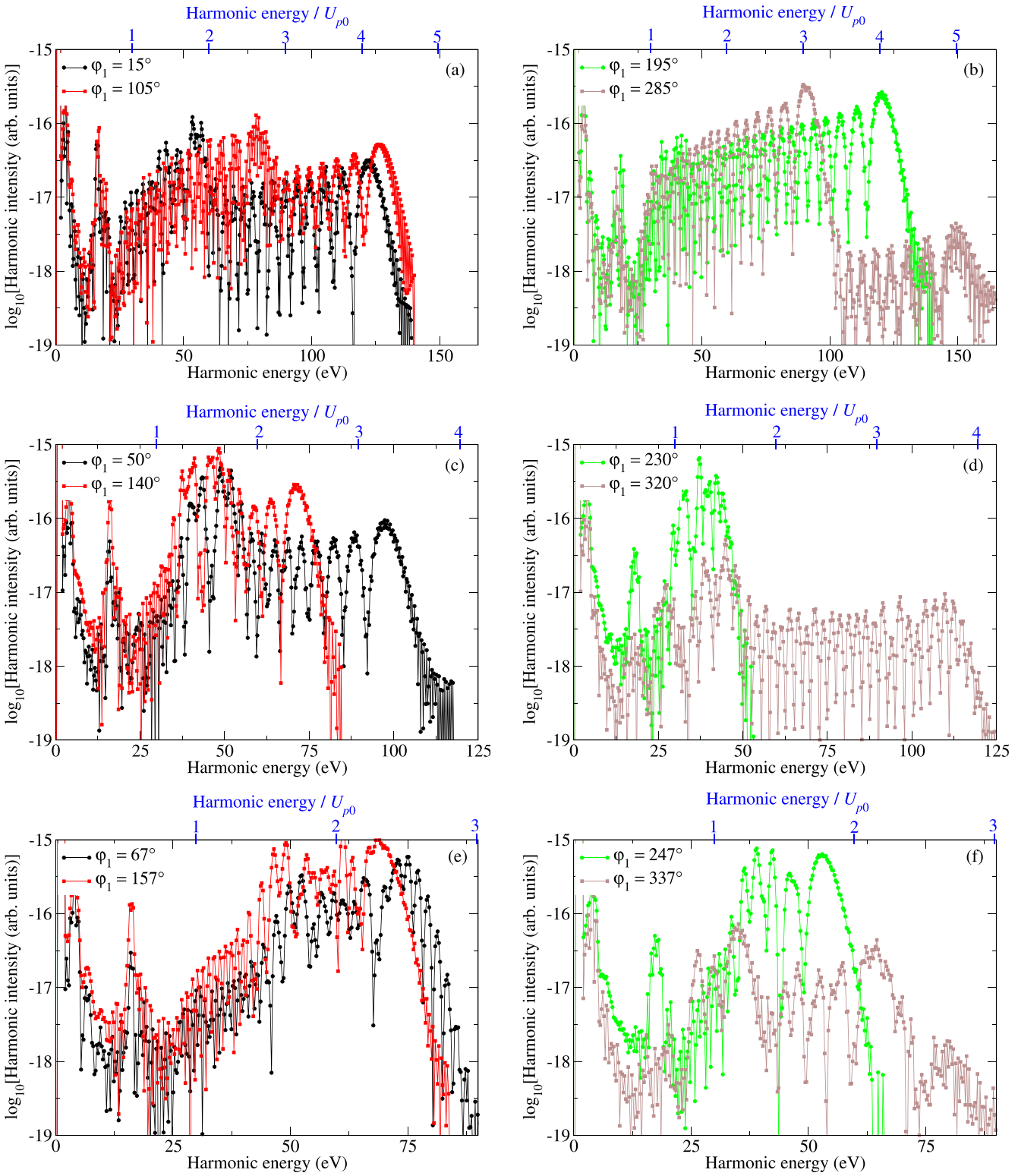

FIG. 9. Logarithm of the harmonic intensity as a function of the harmonic energy for the Ar atom exposed to the ω-2ω linearly polarized field which consists of three optical cycles per pulse and for the values of the absolute phases $\varphi_2 = 0°$ and φ_1 as indicated in the panels. The intensity of the driving-field components is $E_1^2 = E_2^2 = 10^{14}$ W/cm^2, while the fundamental carrier wavelength is 1600 nm.

chosen a longer wavelength in order to obtain a longer plateau and to make the conclusions about the investigated dependences more plausible. The energy scale at the bottom (top) of the panels is in electron volts (U_{p0}). For example, in Figs. 9(a) and 9(b) we compare the harmonic spectra calculated using the driving pulse with $\varphi_1 = 15° + j \times 90°$, $j = 0, 1, 2, 3$. All of these values of the absolute phase would lead to the same harmonic spectrum with the cutoff around $3.2U_{p0}$ (see Fig. 12

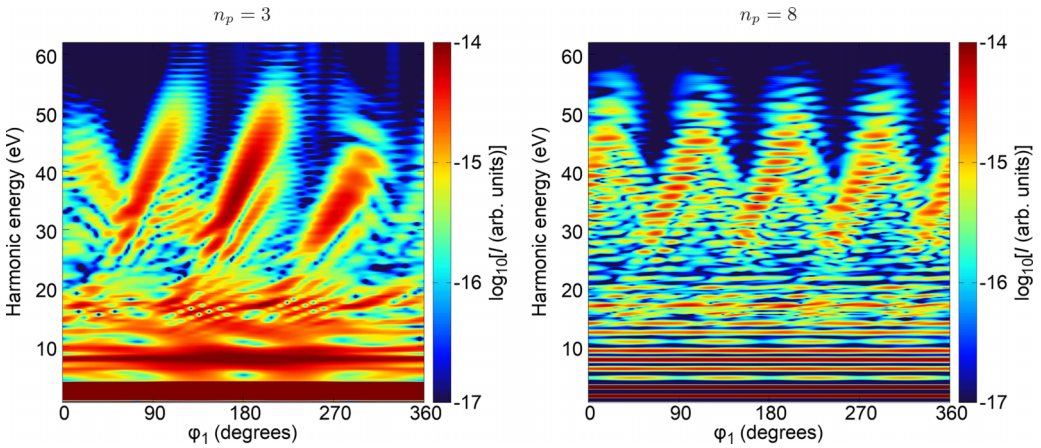

FIG. 10. Logarithm of the harmonic intensity I as a function of the absolute phase φ_1 and the harmonic energy. The intensity of the driving-field components is $E_1^2 = E_2^2 = 10^{14}\,\mathrm{W/cm^2}$, while the fundamental carrier wavelength and the absolute phase φ_2 are 800 nm and 0°, respectively. The number of optical cycles per pulse is indicated above the panels.

in the Appendix) if the long pulse with a flat envelope is employed to induce the process. Moreover, for the case of the long pulse, the harmonic intensity rapidly decreases in the low-energy region, after which it remains, on average, constant for energy lower than 45 eV. Furthermore, for the harmonic energy between 45 and 90 eV, the harmonic intensity is higher than in the previous interval, but still, it is on average constant. None of these characteristics are preserved for the case of a few-cycle pump. In particular, the harmonic intensity and the shape and the length of the spectrum profoundly depend on the absolute phase φ_1. For example, for $\varphi_1 = 15^\circ$ or 105°, the spectra have two plateaus, the one with lower harmonic energy and higher harmonic intensity, and the one with higher harmonic energy and lower harmonic intensity [see the black and red (gray) lines in Fig. 9(a)]. This remains true for the pump pulse with $\varphi_1 = 285^\circ$, with the exceptions that the first plateau is longer than for the pump with $\varphi_1 = 15^\circ$ or 105°, and that the difference between the harmonic intensity of the first and second plateaus is more pronounced [see the brown (gray) line in Fig. 9(b)]. On the other hand, for the phase $\varphi_1 = 195^\circ$, only one plateau appears in the spectrum and the harmonic intensity is high. For all these cases, the position of the cutoff is higher than $4U_{p0}$, i.e., it is much larger than for the pulse with one carrier frequency.

As a second example, in Figs. 9(c) and 9(d) we present the harmonic spectra induced by the driving field with $\varphi_1 = 50^\circ + j \times 90^\circ$, $j = 0, 1, 2, 3$. For these values of the phase φ_1, the position of the harmonic cutoff is close to $5U_{p0}$ (see Fig. 12 in the Appendix) if the long pulse with a flat envelope is employed to induce the process. In addition, the harmonic intensity is on average constant for a broad region of the harmonic energies higher than 30 eV. For a few-cycle pump pulse the situation is different. Not only is the harmonic emission not the same for these values of the absolute phase φ_1, but also the positions of the cutoff are far lower than those obtained with a long pump pulse. For example, for the values $\varphi_1 = 50^\circ, 140^\circ$, and 320°, the cutoff appears at different values of energy between $2U_{p0}$ and $4U_{p0}$, while for $\varphi_1 = 230^\circ$, the position of the cutoff is lower than $1.5U_{p0}$, i.e., always lower than for a long pump pulse. Additionally, the value of the harmonic intensity is different for different values of $\varphi_1 = 50^\circ + j \times 90^\circ$, $j = 0, 1, 2, 3$. Finally, for the long driving pulse with phase $\varphi_1 = 67^\circ + j \times 90^\circ$, $j = 0, 1, 2, 3$, the harmonic spectra exhibit long plateaus (the cutoff energy is higher than $5U_{p0}$) with, on average, constant harmonic intensity (see Fig. 12 in the Appendix). However, for an ultrashort three-cycle pulse, these phases correspond to the pump pulse for which the plateau would be short [see Figs. 9(e) and 9(f)] with the cutoff energy below $2.5U_{p0}$. In summary, the ultrashort nature of the pulse drastically changes the shape and the length of the harmonic plateau.

In conclusion, when an ultrashort pulse is employed to induce the HHG process, the dependence of the harmonic intensity on the phase φ_1 may be completely different with respect to the one obtained using a long pulse with a flat envelope. We will now investigate how short the pulse should be in order that the short-pulse-induced characteristics of the spectra become pronounced. In Fig. 10 we present the logarithm of the harmonic intensity as a function of the absolute phase φ_1 and the harmonic energy for the fixed value $\varphi_2 = 0^\circ$. The intensity of the driving-field components is $E_1^2 = E_2^2 = 10^{14}\,\mathrm{W/cm^2}$, while the fundamental carrier wavelength is 800 nm. The number of optical cycles per pulse is indicated above the panels. For the driving pulse which consists of three optical cycles, the symmetry with respect to the transformation $\varphi_1 \to \varphi_1 + \pi/2$ cannot be observed (see the left panel in Fig. 10). In addition, the harmonic intensity is, on average, a smooth function of the harmonic energy, particularly for the values of the phase for which the harmonic intensity is high. On the other hand, for the eight-cycle driving pulse, the symmetry with respect to the change $\varphi_1 \to \varphi_1 + \pi/2$ becomes apparent (see the right panel in Fig. 10). In addition, for all values of the absolute phase φ_1, the harmonic intensity is an oscillatory function of the harmonic energy. Even though it is generally accepted that a flat envelope is a good approximation for pulses longer than ten optical cycles, we see that the characteristics of the long driving pulse with a flat envelope become apparent even for shorter pulses. For the driving-field intensity and carrier wavelength used for our

example presented in Fig. 10, the short-pulse characteristics are very pronounced for $n_p < 5$.

Similarly as for the HATI process, it is also instructive to analyze the dependence of HHG spectra on the absolute phase φ_2 of the second-harmonic field, with a fixed phase φ_1. In Fig. 11 we display the logarithm of the harmonic intensity as a function of the absolute phase φ_2 and the harmonic energy for the fixed value $\varphi_1 = 0$ and the driving pulse with three optical cycles. The intensity of the driving-field components is $E_1^2 = E_2^2 = 10^{14}\,\mathrm{W/cm^2}$, while the fundamental carrier wavelength is 900 nm. For a long bichromatic driving field with a flat envelope, the HHG spectra depend on the value of the phase φ_2 in such a way that the harmonic yield possesses the symmetry property with respect to the transformation $\varphi_2 \to \varphi_2 + \pi$ (see the Appendix). This symmetry is broken for a few-cycle pump, and the harmonic intensity strongly deviates from that obtained using the long pulse with a flat envelope. For some values of the phase φ_2, the harmonic intensity is lower, while for other values it is higher than the one obtained with a long driving pulse.

The regions in the absolute phase-harmonic energy plane where the harmonic intensity is maximal can be assessed using the one-dimensional simple man's model. In Fig. 11, we added a curve (black line) which corresponds to Eq. (7) and determines the maximal harmonic intensity. This curve nicely follows the region with the maximal harmonic intensity. The simple man's model can be employed to qualitatively assess the regions in the absolute phase-harmonic energy plane in which the harmonic intensity is significant.

In conclusion, an advanced coherent control of the HATI and HHG processes can be achieved using the linearly polarized few-cycle pulse with two carrier frequencies. This control is far more sophisticated than the one accomplished with a linearly polarized few-cycle pulse with one carrier frequency.

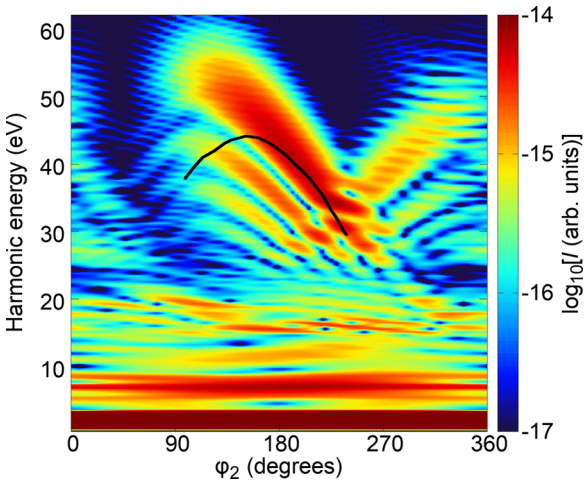

FIG. 11. Logarithm of the harmonic intensity I as a function of the absolute phase φ_2 and the harmonic energy. The intensity of the driving-field components is $E_1^2 = E_2^2 = 10^{14}\,\mathrm{W/cm^2}$, while the fundamental carrier wavelength and the absolute phase φ_1 are 900 nm and 0°, respectively. The number of optical cycles per pulse is $n_p = 3$. The black curve, obtained using the one-dimensional simple man's model, determines the optimal harmonic intensity.

IV. CONCLUSIONS

In recent years, ultrashort pulses which consist of only a few optical cycles per pulse become widely available. The strong-field processes induced by these pulses exhibit many new features in comparison with the scenarios in which the process is induced using a long pulse with a flat envelope. A particularly prominent example of these features is the forward-backward asymmetry present in the photoelectron spectra. The characteristics of the strong-field-induced processes depend on the laser-field parameters which serve as control knobs.

In the first part of our paper, we have analyzed the laser-induced photoelectron emission in high-order above-threshold ionization. In particular, we have investigated the dependence of the photoelectron spectra on the values of the absolute phases of the laser-field components and on the length of the pulse. We have shown that the photoelectron yield depends significantly on the values of the absolute phases. In particular, the position of the cutoff and the photoelectron yield are sensitive to the change of these parameters. The similar conclusions hold for the shape of the spectra. Using the saddle-point method, we have found the partial contributions to the differential ionization probability. Usually, there are two pairs which contribute significantly to the photoelectron yield, one in the high-energy and one in the medium-energy part of the spectrum. Depending on the values of the absolute phases, the contributions of these solutions change. For some values of the absolute phases the high-energy contribution is dominant, while for others, the total spectrum can be reproduced using the medium-energy pair alone. In addition, there are intervals of values of the absolute phases in which both pairs contribute equally to the photoelectron spectra. We have shown that the electron trajectories which correspond to these solutions are qualitatively different. This means that by changing the values of the absolute phases we actually control the electron dynamics in the laser field.

Besides the dependence on the values of the absolute phases, we have also investigated the dependence on the length of the pulse. We have found that the dependence on the absolute phases is significantly changed when the pulse length is changed. This remains true for the pulses shorter than five optical cycles. For longer sine-squared pulses, the spectra resemble the characteristics of those induced by the long pulse with a flat envelope. If the length of the pulse is very short, the values of the absolute phases for which the rescattering part of the photoelectron spectra is suppressed or pronounced strongly depend on the actual length of the pulse. Sometimes, the rescattering part of the spectrum can be completely absent.

In the second part of our paper, we have analyzed the dependence of the high-order harmonic spectra on the parameters of the employed ultrashort pulses. Similarly as for the high-order above-threshold ionization, the harmonic yield induced by a few-cycle sine-squared pulse is radically different from the one generated using a long pulse with a flat envelope. We have analyzed the symmetry properties of the harmonic spectra induced by the long pulse which are broken when an ultrashort pump is employed. We have concluded that the broken symmetry is most pronounced for a very short pulse with duration which covers only a few optical cycles.

When the number of optical cycles per pulse increases, the spectra exhibit oscillatory character as a function of the harmonic energy. We have also illustrated that the regions with large harmonic intensity can successfully be assessed using the simple man's model based on the solution of the Newton equation of motion.

In conclusion, an ultrashort linearly polarized pulse with two carrier frequencies can successfully be used to achieve advanced control over the photoelectron and high-order harmonic spectra and to efficiently control the electron dynamics in the applied field. These pulses can experimentally be created using a two-color Mach-Zehnder interferometer in which the fundamental beam is split into two parts one of which remains unchanged while the frequency of the other is doubled when it passes through a BBO crystal [41,74]. The fundamental beam can have stabilized CEP which is inherited by the second-harmonic beam and the additional relative phase between the two beams can be controlled. Finally, the few-cycle pulses with two carrier frequencies can also be synthesized using two CEP-stabilized, few-cycle optical parametric chirped pulse amplifiers centered at different carrier frequencies [75].

ACKNOWLEDGMENT

We gratefully acknowledge support by the Ministry for Science, Higher Education and Youth of Canton Sarajevo, Bosnia and Herzegovina.

APPENDIX: SYMMETRIES OF THE HHG AND HATI SPECTRA INDUCED BY A TWO-COLOR LINEARLY POLARIZED FIELD

In this Appendix, we investigate the symmetry properties of the HHG and HATI spectra, in the framework of the strong-field approximation, with respect to the change of the phases φ_1 and φ_2 for a long driving pulse with a flat envelope [$f(t) = 1$ in Eq. (8)]. For the long driving pulse with a flat envelope, the integral over time t, which appears in the expressions for the T-matrix element, Eqs. (1), (2), and (5), reduces to the integral over one optical period, i.e., over the interval $[\tau_0, \tau_0 + T]$, where τ_0 is an arbitrary constant time. In addition, since the pulse is long, the upper limit of the integral in Eqs. (2) and (6) can be, after the substitution $\tau = t - t_0$, set to infinity, i.e., $\int_{-\infty}^{t} dt_0 f(t, t_0) \to \int_0^{\infty} d\tau f(t, t-\tau)$. By choosing $\tau_0 = -\varphi_2/(s\omega)$, and using the substitutions $t' = t - \tau_0$ and $t_0' = t_0 - \tau_0$, we get $\int_{\tau_0}^{\tau_0+T} dt \int_0^{\infty} d\tau f(t, t-\tau) = \int_0^{T} dt' \int_0^{\infty} d\tau f(t'+\tau_0, t'+\tau_0-\tau)$, so that $s\omega(t'+\tau_0) + \varphi_2 = s\omega t'$, i.e., the function $f(t'+\tau_0, t'+\tau_0-\tau)$ and the T-matrix elements $\mathbf{T}_{\Omega_\mathbf{K}}$ and $M_{\mathbf{p}m}$ do not depend on the phase φ_2, since $s\omega(t''+\tau_0) + \varphi_2 = s\omega t'', t'' = t', t'-\tau$. Therefore, we can set $\varphi_2 = 0^\circ$ and explore how the T-matrix elements behave as a function of φ_1. Analogously, it is possible to choose $\tau_0 = -\varphi_1/(r\omega)$ and explore the dependence of the T-matrix element on the phase φ_2 alone. For HHG, this type of analysis was performed in [76,77].

Let us denote our field by $\mathbf{E}(t) = E(t, \varphi_1)\hat{\mathbf{e}}_x$ and analyze how the spectra change with respect to the shift of the phase φ_1. The HHG and HATI spectra do not change if the corresponding T-matrix element is invariant with respect to some transformation up to a sign. The translation of the time t does not change the value of the integral and the corresponding T-matrix element. Therefore, in order to investigate how the shift of the phase affects the HATI and HHG spectra, we should find whether such a shift of the time exists that has the same effect on the subintegral function (up to a sign) as the investigated phase transformation.

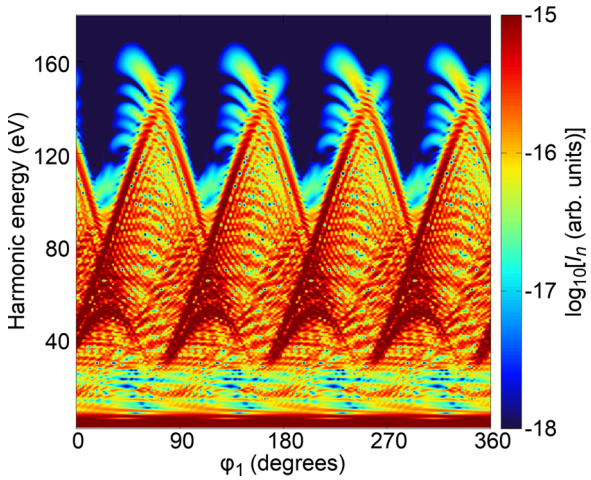

FIG. 12. Logarithm of the harmonic intensity as a function of the absolute phase φ_1 and the harmonic energy ($\varphi_2 = 0^\circ$) for the Ar atom exposed to the ω-2ω long driving field with the component intensity $E_1^2 = E_2^2 = 10^{14}\,\mathrm{W/cm^2}$, and the fundamental wavelength of 1600 nm.

It can be shown that

$$\begin{aligned} E(t, \varphi_1 + \pi) &= -E_1 \sin(r\omega t + \varphi_1) + E_2 \sin(s\omega t), \\ E(t + T/2, \varphi_1) &= (-1)^r E_1 \sin(r\omega t + \varphi_1) \\ &\quad + (-1)^s E_2 \sin(s\omega t) \end{aligned} \tag{A1}$$

with analogous relations for $A(t, \varphi_1)$ and $\alpha(t, \varphi_1)$. Therefore, for r odd and s even we have $E(t, \varphi_1 + \pi) = E(t + T/2, \varphi_1)$, and both the HHG and HATI spectra are invariant with respect to the shift of the phase φ_1 by π. On the other hand, for r even and s odd we have $E(t, \varphi_1 + \pi) = -E(t + T/2, \varphi_1)$. In this case the HHG spectra are invariant, while the HATI spectra are not invariant with respect to the transformation $\varphi_1 \to \varphi_1 + \pi$. The reason is that the subintegral function for HATI contains the term $[\mathbf{p} + \mathbf{A}(t)]^2$. This term changes when the vector potential changes the sign. Only if simultaneously $\mathbf{p} \to -\mathbf{p}$ we have the symmetry $(-\mathbf{p}, \varphi_1 + \pi) \leftrightarrow (\mathbf{p}, \varphi_1)$.

Analogously, for odd $r = 2n + 1, n = 0, 1, 2, \ldots$, it can be shown that

$$E[t, \varphi_1 + (2j+1)\pi/2] = -E[t + (2q+1)T/4, \varphi_1], \tag{A2}$$

for $j + 1 = n + q$ and $s = 4m + 2, m = 0, 1, 2, \ldots$, while

$$E[t, \varphi_1 + (2j+1)\pi/2] = E[t + (2q+1)T/4, \varphi_1], \tag{A3}$$

for $j = n + q$ and $s = 4m + 4$, with j and q integers. In this case, the HHG T-matrix element is invariant (up to a sign) and the corresponding spectrum does not change upon the transformation $\varphi_1 \to \varphi_1 + (2j+1)\pi/2$. An example (for $n = m = 0, q = 1, j = 0$) is shown in Fig. 12. Due to the fact that the phase transformation (A2) changes the sign of the vector potential $A(t, \varphi_1)$ with respect to the time translation

TABLE I. Symmetries of the HHG and HATI spectra with respect to the shift of the $r\omega$-$s\omega$ field phase φ_1 by $\Delta\varphi = \pi/2, \pi$.

r	s	$s/2$	HHG	HATI
Odd	Even	Odd	$\pi/2$	π
Odd	Even	Even	$\pi/2$	$\pi/2$
Even	Odd		π	2π

$t \to t + (2q+1)T/4$ for $s = 4m+2$, the HATI spectra are not invariant. However, the HATI spectra are invariant with respect to the phase transformation (A3), for which $s/2$ is even.

Finally, the most challenging case is when both $r = 2n+1$ and $s = 2m+1$ are odd. In this case, the phase transformation $\varphi_1 \to \varphi_1 + 2\pi/(2k+1)$, $k = 1, 2, \ldots$, can be related with the time translation $t \to t + T/(2k+1)$ for some values of n and m. In particular, in order for the time translation $t \to t + T/(2k+1)$ to induce the same change (up to a sign) as the phase transformation $\varphi_1 \to \varphi_1 + 2\pi/(2k+1)$, it is necessary that the following two pairs of conditions are satisfied:

$$\sin[2\pi(2m+1)/(2k+1)] = 0,$$
$$\cos[2\pi(2m+1)/(2k+1)] = \pm 1, \tag{A4}$$

$$\cos[2\pi/(2k+1)] = \pm\cos[2\pi(2n+1)/(2k+1)],$$
$$\sin[2\pi/(2k+1)] = \pm\sin[2\pi(2n+1)/(2k+1)]. \tag{A5}$$

For every k, we find the integer values of n and m (i.e., of r and s) for which the conditions (A4) and (A5) are satisfied. For the values of r and s such that we have the plus sign in Eqs. (A4) and (A5), both the HHG and HATI spectra are invariant with respect to the phase transformation $\varphi_1 \to \varphi_1 + 2\pi/(2k+1)$, while for the values for which we have the minus sign, the transformation $\varphi_1 \to \varphi_1 + 2\pi/(2k+1)$ is the symmetry transformation only for the HHG spectra. However, it is easy to see that, in the latter case, no integer m satisfies the second condition in (A4). This means that for r and s both odd, both the HHG and HATI spectra possess the same symmetry property. For example, for $k = 1$, the conditions (A4) and (A5) with the plus sign are satisfied for $r = 1, 7, 13, \ldots$ and $s = 3, 9, 15, \ldots$, so that in this case both the HHG and HATI spectra are invariant with respect to the phase transformation $\varphi_1 \to \varphi_1 + 2\pi/3$.

In conclusion, we have shown that, for an $r\omega$-$s\omega$ infinitely long pulse with a flat envelope, for r odd and s even, the HHG spectrum is invariant with respect to the shift of the phase φ_1 by $j\pi/2$, $j = 1, 2, 3$, while the HATI spectrum is invariant with respect to the shift by $\pi/2$ if $s/2$ is even, and with respect to the shift by π if $s/2$ is odd. On the other hand, for r even and s odd we found only the HHG-spectrum symmetry $\varphi_1 \to \varphi_1 + \pi$. These results are summarized in Table I. In the end, for both r and s odd, various symmetries with respect to the phase shift can be present in both the HHG and HATI spectra, depending on the exact values of r and s. For the frequently used ω-3ω field both the HHG and HATI spectra are invariant with respect to the phase transformation $\varphi_1 \to \varphi_1 + 2\pi/3$.

[1] W. Becker, F. Grasbon, R. Kopold, D. B. Milošević, G. G. Paulus, and H. Walther, Above-threshold ionization: From classical features to quantum effects, Adv. At. Mol. Opt. Phys. **48**, 35 (2002).

[2] D. B. Milošević and F. Ehlotzky, Scattering and reaction processes in powerful laser fields, Adv. At. Mol. Opt. Phys. **49**, 373 (2003).

[3] M. C. Kohler, T. Pfeifer, K. Z. Hatsagortsyan, and C. H. Keitel, Frontiers of atomic high-harmonic generation, Adv. At. Mol. Opt. Phys. **61**, 159 (2012).

[4] P. Agostini and L. F. DiMauro, Atomic and molecular ionization dynamics in strong laser fields: From optical to x-rays, Adv. At. Mol. Opt. Phys. **61**, 117 (2012).

[5] S. V. Popruzhenko, Keldysh theory of strong field ionization: History, applications, difficulties and perspectives, J. Phys. B **47**, 204001 (2014).

[6] F. Calegari, G. Sansone, S. Stagira, C. Vozzi, and M. Nisoli, Advances in attosecond science, J. Phys. B **49**, 062001 (2016).

[7] W. Becker, S. P. Goreslavski, D. B. Milošević, and G. G. Paulus, The plateau in above-threshold ionization: The keystone of rescattering physics, J. Phys. B **51**, 162002 (2018).

[8] K. Amini, J. Biegert, F. Calegari, A. Chacón, M. F. Ciappina, A. Dauphin, D. K. Efimov, C. F. de Morisson Faria, K. Giergiel, P. Gniewek *et al.*, Symphony on strong field approximation, Rep. Prog. Phys. **82**, 116001 (2019).

[9] C F. de Morisson Faria and A. S. Maxwell, It is all about phases: Ultrafast holographic photoelectron imaging, Rep. Prog. Phys. **83**, 034401 (2020).

[10] P. B. Corkum, Plasma perspective on strong field multiphoton ionization, Phys. Rev. Lett. **71**, 1994 (1993).

[11] K. J. Schafer, B. Yang, L. F. DiMauro, and K. C. Kulander, Above threshold ionization beyond the high harmonic cutoff, Phys. Rev. Lett. **70**, 1599 (1993).

[12] T. Brabec and F. Krausz, Intense few-cycle laser fields: Frontiers of nonlinear optics, Rev. Mod. Phys. **72**, 545 (2000).

[13] F. Krausz and M. Ivanov, Attosecond physics, Rev. Mod. Phys. **81**, 163 (2009).

[14] G. G. Paulus, F. Grasbon, H. Walther, P. Villoresi, M. Nisoli, S. Stagira, E. Priori, and S. De Silvestri, Absolute-phase phenomena in photoionization with few-cycle laser pulses, Nature (London) **414**, 182 (2001).

[15] D. B. Milošević, G. G. Paulus, and W. Becker, Phase-dependent effects of a few-cycle laser pulse, Phys. Rev. Lett. **89**, 153001 (2002).

[16] F. Grasbon, G. G. Paulus, H. Walther, P. Villoresi, G. Sansone, S. Stagira, M. Nisoli, and S. De Silvestri, Above-threshold ionization at the few-cycle limit, Phys. Rev. Lett. **91**, 173003 (2003).

[17] D. B. Milošević, G. G. Paulus, and W. Becker, High-order above-threshold ionization with few-cycle pulse: A meter of the absolute phase, Opt. Express **11**, 1418 (2003).

[18] A. Gazibegović-Busuladžić, E. Hasović, M. Busuladžić, D. B. Milošević, F. Kelkensberg, W. K. Siu, M. J. J. Vrakking, F. Lépine, G. Sansone, M. Nisoli, I. Znakovskaya, and M. F. Kling, Above-threshold ionization of diatomic molecules by few-cycle laser pulses, Phys. Rev. A **84**, 043426 (2011).

[19] C. P. J. Martiny and L. B. Madsen, Symmetry of carrier-envelope phase difference effects in strong-field, few-cycle ionization of atoms and molecules, Phys. Rev. Lett. **97**, 093001 (2006); **97**, 169903(E) (2006).

[20] V. Roudnev and B. D. Esry, General theory of carrier-envelope phase effects, Phys. Rev. Lett. **99**, 220406 (2007).

[21] A. de Bohan, Ph. Antoine, D. B. Milošević, and B. Piraux, Phase-dependent harmonic emission with ultrashort laser pulses, Phys. Rev. Lett. **81**, 1837 (1998).

[22] A. Baltuška, T. Udem, M. Uiberacker, M. Hentschel, E. Goulielmakis, C. Gohle, R. Holzwarth, V. S. Yakovlev, A. Scrinzi, T. W. Hänsch, and F. Krausz, Attosecond control of electronic processes by intense light fields, Nature (London) **421**, 611 (2003).

[23] V. S. Yakovlev and A. Scrinzi, High harmonic imaging of few-cycle laser pulses, Phys. Rev. Lett. **91**, 153901 (2003).

[24] M. Nisoli, G. Sansone, S. Stagira, S. De Silvestri, C. Vozzi, M. Pascolini, L. Poletto, P. Villoresi, and G. Tondello, Effects of carrier-envelope phase differences of few-optical-cycle light pulses in single-shot high-order-harmonic spectra, Phys. Rev. Lett. **91**, 213905 (2003).

[25] C. A. Haworth, L. E. Chipperfield, J. S. Robinson, P. L. Knight, J. P. Marangos, and J. W. G. Tisch, Half-cycle cutoffs in harmonic spectra and robust carrier-envelope phase retrieval, Nat. Phys. **3**, 52 (2007).

[26] A. D. Bandrauk, S. Chelkowski, D. J. Diestler, J. Manz, and K. J. Yuan, Quantum simulation of high-order harmonic spectra of the hydrogen atom, Phys. Rev. A **79**, 023403 (2009).

[27] K. R. Hamilton, H. W. van der Hart, and A. C. Brown, Pulse-shape control of two-color interference in high-order-harmonic generation, Phys. Rev. A **95**, 013408 (2017).

[28] X. Liu, H. Rottke, E. Eremina, W. Sandner, E. Goulielmakis, K. O. Keeffe, M. Lezius, F. Krausz, F. Lindner, M. G. Schätzel, G. G. Paulus, and H. Walther, Nonsequential double ionization at the single-optical-cycle limit, Phys. Rev. Lett. **93**, 263001 (2004).

[29] X. Liu and C. F. de Morisson Faria, Nonsequential double ionization with few-cycle laser pulses, Phys. Rev. Lett. **92**, 133006 (2004).

[30] G. G. Xin, D. F. Ye, and J. Liu, Dependence of the correlated-momentum patterns in double ionization on the carrier-envelope phase and intensity of a few-cycle laser pulse, Phys. Rev. A **82**, 063423 (2010).

[31] T. Shaaran, C. F. de Morisson Faria, and H. Schomerus, Causality and quantum interference in time-delayed laser-induced nonsequential double ionization, Phys. Rev. A **85**, 023423 (2012).

[32] C. F. de Morisson Faria, T. Shaaran, and M. T. Nygren, Time-delayed nonsequential double ionization with few-cycle laser pulses: Importance of the carrier-envelope phase, Phys. Rev. A **86**, 053405 (2012).

[33] M. F. Kling, Ch. Siedschlag, A. J. Verhoef, J. I. Khan, M. Schultze, Th. Uphues, Y. Ni, M. Uiberacker, M. Drescher, F. Krausz, and M. J. J. Vrakking, Control of electron localization in molecular dissociation, Science **312**, 246 (2006).

[34] D. Ray, F. He, S. De, W. Cao, H. Mashiko, P. Ranitovic, K. P. Singh, I. Znakovskaya, U. Thumm, G. G. Paulus, M. F. Kling, I. V. Litvinyuk, and C. L. Cocke, Ion-energy dependence of asymmetric dissociation of D_2 by a two-color laser field, Phys. Rev. Lett. **103**, 223201 (2009).

[35] A. Čerkić and D. B. Milošević, Few-cycle laser-pulse-assisted electron-atom potential scattering, Phys. Rev. A **87**, 033417 (2013).

[36] A. Čerkić and D. B. Milošević, Few-cycle-laser-pulse-assisted electron-ion radiative recombination, Phys. Rev. A **88**, 023414 (2013).

[37] M. Busuladžić, A. Čerkić, S. Odžak, A. Gazibegović-Busuladžić, E. Hasović, D. Habibović, and D. B. Milošević, Atomic and molecular processes generated by linearly polarized few-cycle laser pulses, Phys. Scr. **T162**, 014008 (2014).

[38] B. Fetić and D. B. Milošević, Carrier-envelope-phase control of plasmonic-field enhanced high-order harmonic generation, J. Mod. Opt. **60**, 1466 (2013).

[39] D. Habibović, W. Becker, and D. B. Milošević, Symmetries and selection rules of the spectra of photoelectrons and high-order harmonics generated by field-driven atoms and molecules, Symmetry **13**, 1566 (2021).

[40] T. Rook and C. F. de Morisson Faria, Exploring symmetries in photoelectron holography with two-color linearly polarized fields, J. Phys. B **55**, 165601 (2022).

[41] D. G. Arbó, C. Lemell, S. Nagele, N. Camus, L. Fechner, A. Krupp, T. Pfeifer, S. D. López, R. Moshammer, and J. Burgdörfer, Ionization of argon by two-color laser pulses with coherent phase control, Phys. Rev. A **92**, 023402 (2015).

[42] N. Douguet, A. N. Grum-Grzhimailo, and K. Bartschat, Above-threshold ionization in neon produced by combining optical and bichromatic XUV femtosecond laser pulses, Phys. Rev. A **95**, 013407 (2017).

[43] D. Peng, L.-W. Pi, M. V. Frolov, and A. F. Starace, Enhancing high-order-harmonic generation by time delays between two-color, few-cycle pulses, Phys. Rev. A **95**, 033413 (2017).

[44] S. D. López, S. Donsa, S. Nagele, D. G. Arbó, and J. Burgdörfer, Phase delays in ω-2ω above-threshold ionization, Phys. Rev. A **104**, 043113 (2021).

[45] W. Hu, X. Li, H. Zhao, W. Li, Y. Lei, X. Kong, A. Liu, S. Luo, and D. Ding, Sub-optical-cycle electron dynamics of NO molecules: The effect of strong laser field and Coulomb field, J. Phys. B **53**, 084002 (2020).

[46] G. Duchateau, A. Yamada, and K. Yabana, Electron dynamics in a-quartz induced by two-color 10-femtosecond laser pulses, Phys. Rev. B **105**, 165128 (2022).

[47] A. C. Brown, G. S. J. Armstrong, J. Benda, D. D. A. Clarke, K. R. Hamilton, Z. Mašín, J. D. Gorfinkiel, and H. W. van der Hart, RMT: R-matrix with time-dependence. Solving the semi-relativistic, time-dependent Schrödinger equation for general, multielectron atoms and molecules in intense, ultrashort, arbitrarily polarized laser pulses, Comput. Phys. Commun. **250**, 107062 (2020).

[48] B. Fetić, W. Becker, and D. B. Milošević, Extracting photoelectron spectra from the time-dependent wave function: Comparison of the projection onto continuum states and window-operator methods, Phys. Rev. A **102**, 023101 (2020).

[49] X.-Y. Lai, C. Poli, H. Schomerus, and C. F. de Morisson Faria, Influence of the Coulomb potential on above-threshold ionization: A quantum-orbit analysis beyond the strong-field approximation, Phys. Rev. A **92**, 043407 (2015).

[50] A. S. Maxwell and C. F. de Morisson Faria, Coulomb-free and Coulomb-distorted recolliding quantum orbits in photoelectron holography, J. Phys. B **51**, 124001 (2018).

[51] L. Cruz Rodriguez, T. Rook, B. B. Augstein, A. S. Maxwell, and C. F. de Morisson Faria, Forward and hybrid path-integral methods in photoelectron holography: Sub-barrier corrections, initial sampling, and momentum mapping, Phys. Rev. A **108**, 033114 (2023).

[52] T. Rook, D. Habibović, L. Cruz Rodriguez, D. B. Milošević, and C. F. de Morisson Faria, Impact of the continuum Coulomb interaction in quantum-orbit-based treatments of high-order above-threshold ionization, Phys. Rev. A **109**, 033115 (2024).

[53] D. B. Milošević and W. Becker, Improved strong-field approximation and quantum-orbit theory: Application to ionization by a bicircular laser field, Phys. Rev. A **93**, 063418 (2016).

[54] D. B. Milošević and W. Becker, X-ray harmonic generation by orthogonally polarized two-color fields: Spectral shape and polarization, Phys. Rev. A **100**, 031401(R) (2019).

[55] D. Habibović and D. B. Milošević, Ellipticity of high-order harmonics generated by aligned homonuclear diatomic molecules exposed to an orthogonal two-color laser field, Photonics **7**, 110 (2020).

[56] D. Habibović, A. Gazibegović-Busuladžić, M. Busuladžić, A. Čerkić, and D. B. Milošević, Strong-field ionization of homonuclear diatomic molecules using orthogonally polarized two-color laser fields, Phys. Rev. A **102**, 023111 (2020).

[57] D. Habibović and D. B. Milošević, Above-threshold detachment by strong ultrashort two-component laser pulses, Phys. Rev. A **107**, 053110 (2023).

[58] D. Habibović and D. B. Milošević, Phase-dependent effects in strong-field ionization induced by a two-component ultrashort laser pulse, Eur. Phys. J. D **78**, 8 (2024).

[59] D. B. Milošević, D. Bauer, and W. Becker, Quantum-orbit theory of high-order atomic processes in intense laser fields, J. Mod. Opt. **53**, 125 (2006).

[60] D. Bauer, D. B. Milošević, and W. Becker, On the validity of the strong field approximation and simple man's theory, J. Mod. Opt. **53**, 135 (2006).

[61] D. B. Milošević, G. G. Paulus, D. Bauer, and W. Becker, Above-threshold ionization by few-cycle pulses, J. Phys. B **39**, R203 (2006).

[62] A. A. Radzig and B. M. Smirnov, *Reference Data on Atoms, Molecules, and Ions* (Springer-Verlag, Berlin, 1985).

[63] A. E. S. Green, D. E. Rio, and T. Ueda, Analytic velocity-dependent potential for bound and scattering states of electrons and atoms, Phys. Rev. A **24**, 3010 (1981).

[64] D. B. Milošević, A. Čerkić, B. Fetić, E. Hasović, and W. Becker, Low-frequency approximation for high-order above-threshold ionization, Laser Phys. **20**, 573 (2010).

[65] X. M. Tong and C. D. Lin, Empirical formula for static field ionization rates of atoms and molecules by lasers in the barrier-suppression regime, J. Phys. B **38**, 2593 (2005).

[66] D. B. Milošević, Circularly polarized high harmonics generated by a bicircular field from inert atomic gases in the p state: A tool for exploring chirality-sensitive processes, Phys. Rev. A **92**, 043827 (2015).

[67] H. G. Muller and H. B. van Linden van den Heuvell, Limiting cases of excess-photon ionization, in *Multiphoton Processes: Proceedings of ICOMP 4*, edited by S. J. Smith and P. L. Knight (Cambridge University, London, 1988), pp. 25–34.

[68] T. F. Gallagher, Above-threshold ionization in low-frequency limit, Phys. Rev. Lett. **61**, 2304 (1988).

[69] P. B. Corkum, N. H. Burnett, and F. Brunel, Above-threshold ionization in the long-wavelength limit, Phys. Rev. Lett. **62**, 1259 (1989).

[70] G. G. Paulus, W. Becker, W. Nicklich, and H. Walther, Rescattering effects in above-threshold ionization: a classical model, J. Phys. B **27**, L703 (1994).

[71] D. B. Milošević and W. Becker, Role of long quantum orbits in high-order harmonic generation, Phys. Rev. A **66**, 063417 (2002).

[72] D. B. Milošević, G. G. Paulus, and W. Becker, Ionization by few-cycle pulses: Tracing the electron orbits, Phys. Rev. A **71**, 061404(R) (2005).

[73] P. Salières, B. Carré, L. Le Déroff, F. Grasbon, G. G. Paulus, H. Walther, R. Kopold, W. Becker, D. B. Milošević, A. Sanpera, and M. Lewenstein, Fewnman's path-integral approach for intense-laser–atom interactions, Science **292**, 902 (2001).

[74] F. Schlaepfer, M. Volkov, N. Hartmann, A. Niedermayr, Z. Schumacher, L. Gallmann, and U. Keller, Phase stabilization of an attosecond beamline combining two IR colors, Opt. Express **27**, 22385 (2019).

[75] S.-W. Huang, G. Cirmi, J. Moses, K.-H. Hong, S. Bhardwaj, J. R. Birge, L.-J. Chen, E. Li, B. J. Eggleton, G. Cerullo, and F. X. Kärtner, High-energy pulse synthesis with sub-cycle waveform control for strong-field physics, Nat. Photon. **5**, 475 (2011).

[76] D. B. Milošević and B. Piraux, High-order harmonic generation in a bichromatic elliptically polarized laser field, Phys. Rev. A **54**, 1522 (1996).

[77] C. F. de Morisson Faria, D. B. Milošević, and G. G. Paulus, Phase-dependent effects in bichromatic high-order harmonic generation, Phys. Rev. A **61**, 063415 (2000).